SLAC-PUB-4362
LBL-23707
October 1987
(T/E)

MEASUREMENT OF THE TAU LIFETIME*

D. Amidei,[a] G. H. Trilling, G. S. Abrams, A. R. Baden,[b] J. Boyer, F. Butler, G. Gidal, M. K. Gold, G. Goldhaber, L. Golding,[c] J. Haggerty,[d] D. Herrup, I. Juricic, J. A. Kadyk, M. E. Nelson,[e] P. C. Rowson,[f] H. Schellman,[a] W. B. Schmidke, P. D. Sheldon,[g] C. de la Vaissiere,[h] and D. R. Wood

Lawrence Berkeley Laboratory and Department of Physics
University of California, Berkeley, California 94720

J. A. Jaros, T. Barklow, A. M. Boyarski, P. Burchat,[i]
D. L. Burke, J. M. Dorfan, G. J. Feldman, L. Gladney,[j]
G. Hanson, K. Hayes, R. J. Hollebeek,[j] W. R. Innes, D. Karlen,
S. R. Klein, A. J. Lankford, R. R. Larsen, B. W. LeClaire,
M. E. Levi, N. S. Lockyer,[j] V. Lüth, C. Matteuzzi,[k]
R. A. Ong, M. L. Perl, B. Richter, K. Riles, and J. M. Yelton[l]

Stanford Linear Accelerator Center
Stanford University, Stanford, California 94305

T. Schaad[m]

Department of Physics, Harvard University
Cambridge, Massachusetts 02138

Submitted to *Physical Review D*

---

* This work was supported in part by the Department of Energy, Contracts DE-AC03-76SF00098 (LBL), DE-AC03-76SF00515 (SLAC), and DE-AC02-76ER03064 (Harvard).

a Present address: Univ. of Chicago, Chicago, IL 60637
b Present address: Harvard Univ., Cambridge, MA 02138
c Present address: Therma-Wave Corp., Fremont, CA 94539
d Present address: Brookhaven National Laboratory, Upton, NY 11973
e Present address: California Institute of Technlogy, Pasadena, CA 91125
f Present address: Columbia University, New York, NY 10027
g Present address: Univ. of Illinois, Urbana IL 61801
h Present address: LPNHE, Univ. Pierre et Marie Curie, F-75230 Paris, France
i Present address: Univ. of California, Santa Cruz, CA 95064
j Present address: Univ. of Pennsylvania, Philadelphia, PA 19104
k Present address: CERN, CH-1211, Geneva 23, Switzerland
l Present address: Oxford University, Oxford, England
m Present address: Univ. of Geneva, CH-1211 Geneva 4, Switzerland

Measurement of the Tau Lifetime

Abstract

We have used a high-resolution drift chamber in the Mark II Detector at the PEP storage ring to measure the lifetime of τ leptons produced in e^+e^- annihilations at 29 GeV. Based on the flight path distribution of 807 3-prong τ decays, the lifetime is found to be $(2.88 \pm 0.16 \pm 0.17) \times 10^{-13}$ sec., in agreement with expectations for e-μ-τ universality.

1. Introduction

In the decade since its discovery, the τ lepton has been extensively studied and is now considered to be a member of a conventional weak doublet, with its own neutrino, and its own conserved lepton number. This third generation lepton thus becomes a laboratory for precision tests of the Standard Model. In this paper we report our measurement of the τ lifetime using data recorded by the Mark II detector at the e^+e^- colliding beam facility PEP.

If the τ couples to the weak charged current with the same strength as the other leptons, its decay rate to electrons can be calculated analogously to muon decay:

$$\Gamma(\tau \to e\, \nu_e\, \nu_\tau) = \frac{G_F^2\, m_\tau^5}{192\, \pi^3}$$

where G_F is the universal Fermi coupling strength, m_τ is the τ mass, and the ν_τ-mass has been neglected. The effect of a ν_τ mass at the present experimental upper bound is negligible compared to other uncertainties in

this analysis.[1] Radiative corrections are also small.[2] The τ lifetime is simply related to this width through the electron branching fraction

$$\tau_\tau = \frac{B(\tau \to e\, \nu_e\, \nu_\tau)}{\Gamma(\tau \to e\, \nu_e \nu_\tau)}$$

Using the experimentally determined branching fraction [3] $(17.9 \pm 0.4)\%$, and mass [4] (1784 ± 3) MeV/c^2, one predicts:

$$\tau_\tau = (2.85 \pm 0.06) \times 10^{-13} \text{ sec}$$

The magnitude of the uncertainty in this prediction is entirely due to the experimental error of the measured electron branching fraction.

The τ lifetime provides an unequivocal test of μ-τ universality. In the Standard Model, all generations couple equally to the same gauge bosons, and e-μ-τ universality is exact.[5] Deviations from universality can arise from mixing in the neutrino sector, or from other new physics.[6] The most stringent limit on e-μ universality comes from the ratio of the π branching fractions to e and μ, which implies that, at the 95% confidence level, the Fermi couplings of these particles to the charged weak current are identical to within 2%.[7] Recently reported measurements of the τ lifetime indicate that the τ Fermi coupling must lie within 10% of the same value.[8] The lifetime measurement presented here includes refinements and extensions of earlier Mark II results,[9] and supersedes them.

2. Experimental procedure

The τ leptons for this analysis are produced in the annihilation of 14.5 GeV electrons and positrons from the PEP storage ring at SLAC. Neglecting small radiative corrections, the $\tau^+\tau^-$ are produced

monochromatically at the beam energy. The τ lifetime is determined from measurement of the mean decay length:

$$\langle l \rangle = \gamma \beta c \tau_\tau$$

To determine the decay length, we use the 3-prong decay mode of the τ to reconstruct a decay vertex, and measure the displacement of this vertex from the beam spot. When radiative corrections to the τ energy are included, the mean pathlength corresponding to the predicted τ lifetime is 660 μm. Good precision in the measurement thus requires high-resolution charged particle tracking, a well measured beam position, and careful consideration of systematic errors.

2.1 Apparatus

The full details of the Mark II detector at PEP have been given elsewhere.[10] We review here those aspects of the tracking system that are particularly relevant to this analysis.

Charged particle tracking in the Mark II is carried out with a combination of two cylindrical drift chambers operating in a solenoidal magnetic field of 2.3 kG, all concentric with the beam line. The main drift chamber (DC)[11] contains 16 equally spaced layers of drift cells at radii between 41 and 145 cm. Six of these layers contain axial sense wires; in the other ten, the sense wires are at $\pm 3^\circ$ to provide stereo information. The position resolution is approximately 200 μm per layer.

In the space between the beam vacuum pipe and the inner wall of the main drift chamber is a smaller high resolution device, known as the vertex chamber (VC).[12] This cylindrical chamber, 1.2 m in length and 0.70 m in diameter, operates with seven layers of drift cells strung between 5 cm

thick aluminum endplates. To minimize the error due to multiple Coulomb scattering, the inner shell is made from beryllium, and serves as the beam pipe. Amounting to only 0.6% of a radiation length, it is the only material between the interaction point and the first vertex chamber position measurement.

The wire array is composed of alternating cathode only and cathode/sense layers, all strung parallel to the beam axis. Sense wires are located to 15 μm accuracy with individual nylon feedthroughs. The radial distance between layers, 4.2 mm, and the distance between adjacent wires at the same radius, 5.3 mm, specify a pattern of roughly hexagonal drift cells. Four layers of inner drift cells lie just outside the beam pipe, at radii from 10.1 to 12.6 cm, and another three layers are clustered at radii from 30.4 to 32.0 cm. In all, there are 270 drift cells in the inner layers and 555 drift cells in the outer.

The chamber operates with a 50/50 mixture of argon-ethane, plus 0.4% ethyl alcohol.[13] At our standard discriminator setting of 200 μV, the chamber is fully efficient at 1.950 kV; our operating voltage is somewhat above this, at 2.10 kV. The resolution of the electronics used for the drift time measurement is approximately 250 psec.

2.2. Offline Reconstruction and Tracking

The first step in offline data reconstruction is the determination of the geometric placement of the vertex detector relative to the main drift chamber. We use a right-handed coordinate system centered in the DC, with positive z axis parallel to the electron beam. The VC position is characterized in terms of 3 small Cartesian rotations, and 2 small

displacements in x and y; the constants are found by least squares minimization of the tracking χ^2 in both chambers for a large ensemble of tracks from Bhabha scattering. The resultant geometry is used as a starting point in a separate algorithm to find the space-time relation in the VC, and this two-step process is repeated until it converges.

The electron drift velocity is saturated throughout the VC drift cell. This ensures a space-time relation which is approximately linear over most of the drift region. The constant spacing between sense and field wires at the same radius allows the use of a single such relation for all drift cells. We use the Bhabha track sample to fit the space-time relation to a third order polynomial, and find significant deviations from linearity only very near and very far from the sense wire. Attempts to use separate relations for those special regions yield no significant improvement in resolution.

To determine track parameters, a least squares fit to drift times in both vertex and main drift chambers is made. Precise angular and position measurements in the x-y plane are supplied by the VC, while dip and curvature information is provided by the DC. To take account of geometric uncertainties in the DC and in the relative VC-DC geometry, we allow small VC-DC relative shifts in the x-y position (σ = 200 μm) and in azimuth (σ=0.3 mr) in the fits. In Fig. 1 we show the distribution of χ^2 constructed from VC residuals on Bhabha tracks with measurements in all seven layers, using an average resolution of 95 μm per layer. Since our fit effectively uses the VC information to determine two parameters (x-y position and slope), we expect a χ^2 distribution appropriate to five

degrees of freedom. This distribution is also plotted in Fig. 1 and, except for the tails, describes the data well.

The position precision of tracks reconstructed in the VC-DC system has been discussed in detail by Gladney et al.[14] From the measured tracking residuals in the vertex detector, and the known scattering contributions, the track position resolution in the x-y plane, extrapolated to the beam center, is predicted to be

$$\sigma_0\,(\mu m) = \sqrt{(85)^2 + (95/P(Gev/c))^2}$$

The first term measures the intrinsic tracking performance, and the second measures the effect of multiple Coulomb scattering. We have verified this prediction with a large sample of Bhabha scattering events. Ignoring multiple Coulomb scattering in this case, we expect the RMS separation distance of the two tracks at the origin to be just $\sqrt{2}$ times the intrinsic resolution there, or 120 μm. The measured distribution of these separation distances, shown in Fig. 2, has an RMS width of 124 μm. Additional studies with Bhabha tracks have also demonstrated the absence of any azimuthal dependence of track parameters measured at the beam center.[14]

2.3 Beam Size and Position

The position and shape of the luminous region are necessary ingredients in the determination of the τ path length. The beam position is derived from a measurement of the average intersection point of Bhabha tracks whose directions, projected into the x-y plane, lie within 100 mr of the vertical and horizontal axes. The average beam position measured in this way is accurate to 20 μm, and is found to be reasonably stable from

one storage ring fill to the next. The beam size is derived from the distribution of Bhabha track impact parameters relative to the measured beam center, corrected for the VC resolution. The result from a fraction of our data is [15]

$$\sigma_{bx} = 481 \pm 18\ \mu m \quad \text{and} \quad \sigma_{by} = 62 \pm 9\ \mu m$$

Further detail on beam position measurement and monitoring can be found in Ref. 14.

3. Selection of the Tau Sample

Tau pair production at 29 GeV center of mass energy has a distinctive signature and can be isolated with little background. Candidate events are subjected to quality cuts to insure the reliability of the tracking information. This analysis is based on data recorded at PEP over a period from 1981 to 1984, with an integrated luminosity of 206 pb^{-1}.

3.1 Event Selection

With the exception of a very small branching fraction to 5 prongs, all τ decay modes produce either 1 or 3 charged tracks in the final state.[16] Our sample of 3-prong decays is selected from events with zero total charge which contain either a pair of 3-prong jets in opposite hemispheres or a single track and a 3-prong jet in opposite hemispheres. To ensure that the event originates in an e^+e^- collision we require that the overall event vertex lie within 2 cm of the beam center in the x-y plane, and within 5 cm along the beam axis.

Further cuts are applied to this sample to minimize anticipated backgrounds. We require that each 3-prong candidate have charge ± 1 and an invariant mass, based on the charged particles, between 0.7 GeV/c^2 and 1.5

GeV/c^2. In addition, we calculate the mass of the tau-like system including nearby neutral energy recorded by the liquid argon calorimeter and require that it be less than 2.0 GeV/c^2. In two jet (6-prong) events, failure of either jet results in the exclusion of both.

Tau pairs produced in the two-photon collision process $e^+e^- \rightarrow e^+e^-\tau^+\tau^-$ are rejected through the requirement that the total charged energy in the event exceed 5.0 GeV, and that the energy of each 3-prong exceed 3.0 GeV. We suppress these events because their τ energies are substantially less than the beam energy, and not well determined.

Finally, we must protect against radiative Bhabha and $\mu^+\mu^-$ events which can mimic the 3 + 1 topology if the photon converts to an electron-positron pair. We therefore require that the total charged energy in each event be less than $0.9E_{cm}$, and that the 3-particle invariant mass, calculated assuming that all tracks are electrons, exceed 300 MeV/c^2.

3.2 Backgrounds

The level of the remaining background in this sample has been studied by Monte Carlo simulation. The Monte Carlo includes accurate representation of VC and DC resolutions, multiple Coulomb scattering in the beam pipe, chamber wires, and VC-DC interface, nuclear scattering and absorption in the beam pipe, pion and kaon decay, photon conversions, and the pattern of inefficient drift cells in the two chambers.

The hadronic event sample is generated using the Feynman-Field fragmentation model and known heavy quark parameters. The magnitude of hadronic backgrounds satisfying our cuts is estimated to be 4.0 ± 0.9 % of the candidate event sample. As a rough check on the simulation, we have

studied real 4 and 6 prong hadronic events with tau-like topologies satisfying the 3 pion mass cuts:

$$2\ \mathrm{Gev}/c^2 < M(3\pi) < 4\ \mathrm{GeV}/c^2$$

$$2\ \mathrm{Gev}/c^2 < M(3\pi+\mathrm{neutrals}) < 4\ \mathrm{GeV}/c^2$$

The number of such events satisfying our τ selection criteria (except for the 3π mass cuts) is found to be 3 in the data and is expected to be 4 from the Monte Carlo. Because of the poor statistics, we assign a 50% uncertainty to the hadronic background, which we take to be 4 ± 2 %.

Two-photon τ production is estimated from a Monte Carlo simulation which generates τ pairs from 2γ collisions via the double equivalent photon approximation. After applying all of the event and track cuts, we find a background from this source of 3.0 ± 1.0 %.

Both of these background estimates include a correction for the somewhat higher efficiency for track finding in the Monte Carlo relative to real data.

Backgrounds from radiative QED processes are found to be negligible and we place an upper limit of 1% on such contributions.

3.3 Track Quality Cuts

The selection outlined in Sec 3.1 yields 1786 3-prong decay candidates. We apply to this sample a further set of tracking quality cuts to ensure that the decay point is well measured. To guarantee a good curvature determination, we require each track to have 6 or more measurements in the main drift chamber. To ensure a good extrapolation to the origin, we require at least two measurements in the VC inner layers and at least one in the VC outer layers. To reduce multiple Coulomb scattering

and the probability of nuclear scattering, we require that the momentum of each of the three tracks exceed 400 MeV/c^2.

We have studied the tracking χ^2 for the VC information alone, and find that tracks from τ events have an average resolution per layer about 15% larger than that inferred from Bhabha scattering events as discussed in Sec. 2.2. The cause has been traced to channel-to-channel cross-talk which occurs in the electronics when tracks are close together in the chamber.[17] We therefore refit all 3-prong tracks with the VC errors increased by 15%. In Fig. 3, we compare the χ^2 distribution for tracks fit in this manner to the expected form. The sample is limited to tracks with 7 VC measurements and, as discussed in Sec. 2.2, the anticipated curve is for 5 degrees of freedom. Again, there is good agreement, except for the tails, and we conclude that the VC resolution in these events is reasonably well understood. For each accepted decay in our sample, we require that all 3 tracks have a VC χ^2 less than 5.0 per degree of freedom, and a χ^2 for the full fit in both chambers of less than 4.0 per degree of freedom.

The application of the above cuts reduces the sample to 1296 passing decays.

4. Determination of the Tau Lifetime

4.1 Vertex Determination

The most probable location of the τ decay point in the plane perpendicular to the beam is found by a one-constraint, least-squares fit to the high precision tracking information in that plane. Measurement and multiple scattering errors in all of the track parameters are taken into

account, and the output of the vertexing calculation includes the (x,y) coordinates of the best fit decay point, the corresponding errors, and the χ^2 of the fit. The distribution of this χ^2 is shown in Fig. 4. To reduce the probability that one or more of the tracks undergo large scattering in the beam pipe, only those events with vertex $\chi^2 < 4.0$ are accepted. An additional consistency check is based on the much less accurate z coordinates of the τ secondaries at the best fit (x,y) decay point. We define the quantity χ^2_z:

$$\chi^2_z = \sum_{i=1}^{3} \frac{(z_i - z_{av})^2}{\sigma^2_{z_i}}$$

where z_{av} is the mean z coordinate of the three tracks, and σ_{zi} the calculated error of the z coordinate of the ith track. The distribution of χ^2_z is expected to correspond to 2 degrees of freedom. The experimental distribution is somewhat broader, and a rather loose cut at $\chi^2_z < 20$ is made. It should be emphasized that the decay point (x,y) coordinates depend almost exclusively on the vertex chamber measurements, with the role of the less precise main drift chamber being to provide the curvature information needed for track extrapolations.

4.2 The τ Decay Length

We now consider, for each event, the optimal estimate of the τ decay length. The situation for a typical event is summarized in Fig. 5, which shows a magnified view near the interaction region, and indicates the beam ellipse as well as the decay vertex error ellipse. We have already discussed the beam ellipse, which is taken to have a position and size as

described in Sec. 2.3. The vertex error ellipse is obtained from the vertex calculation discussed in the previous section. We approximate the (x,y) component of the τ direction by the projection of the vector sum of the momenta of the three charged secondaries. This approximation neglects the effect on the τ direction of the final state neutrino and any π^0 secondary. The error thereby introduced is small and will be discussed later. Taking this approximate τ direction as fixed, we make a one-constraint fit to obtain the best estimates of the production and decay points, and the corresponding decay length. The two dimensional decay length and its error are given by

$$l' = \frac{x_v\sigma_{yy}t_x + y_v\sigma_{xx}t_y - \sigma_{xy}(x_v t_y + y_v t_x)}{\sigma_{yy}t_x^2 + \sigma_{xx}t_y^2 - 2\sigma_{xy}t_x t_y}$$

$$\sigma_l' = \left[\frac{\sigma_{xx}\sigma_{yy} - \sigma_{xy}^2}{\sigma_{yy}t_x^2 + \sigma_{xx}t_y^2 - 2\sigma_{xy}t_x t_y} \right]^{1/2}$$

where (x_v, y_v) are decay vertex positions relative to the center of the beam ellipse, $(\sigma_{xx}, \sigma_{xy}, \sigma_{yy})$ are error matrix elements obtained by adding vertex and beam position error matrices, and (t_x, t_y) are the two-dimensional direction cosines of the τ line of flight.

The two-dimensional quantities l' and σ_l' are converted to three dimensional l and σ_l through division by $\sin\theta_\tau$, where θ_τ is the polar angle of the 3π momentum direction. The distribution of σ_l is shown in Fig. 6. To insure a sample with maximal signal to noise ratio, we retain only those decays for which $\sigma_l < 1.4$ mm, and also require that the τ production point

derived from the above fit be within 2 standard deviations of the measured beam center.

Our final sample, which passes all cuts up to this point, contains 807 decays.

4.3 Maximum likelihood analysis

We construct a likelihood function

$$L = \prod_{i=1}^{N} P_i(l_i, l_\tau)$$

where l_τ is the mean τ decay length that we wish to determine and l_i is the measured decay length for the ith event. The individual event probability P_i is given by the convolution of the exponential decay distribution with a Gaussian resolution function:

$$P_i(l_i, l_\tau) = \frac{1}{l_\tau} \frac{1}{\sqrt{2\pi\sigma_i^2}} \int_0^\infty \exp(-x/l_\tau) \exp\left[-(x-l_i)^2/2\sigma_i^2\right] dx$$

where σ_{li} is the calculated error in l_i. The best fit value of l_τ is obtained by maximization of L.

There is an important subtlety in the application of this procedure to the τ decay length data. As seen from Fig. 6, the typical values of σ_i are comparable in magnitude to the anticipated value of l_τ. As a consequence of this relation, the result of the likelihood fit is sensitive to the values of σ_i. Indeed, the RMS width of the distribution of l_i is easily shown to be

$$\langle (l_i - l_\tau)^2 \rangle = \sigma_i^2 + l_\tau^2$$

The width information is used in the likelihood fit, and any underestimate of σ_i will be compensated by an upward bias in the fitted value of l_τ. Our calculated values of σ_i are, indeed, likely to be underestimates, since various non-Gaussian tails are not included. To avoid this difficulty, at the cost of slightly increased statistical errors, we include in our fit an additional parameter, R, which scales all of the calculated errors as

$$\sigma_i \rightarrow R \cdot \sigma_i$$

By introducing R as a free parameter, we effectively base the determination of l_τ on an appropriately weighted mean value of the individual l_i, rather than on the detailed shape of the l_i distribution.

4.4 Determination of the Tau Lifetime

The distribution of decay lengths for the sample of 807 three prong decays which pass all of the cuts described in previous sections is shown in Fig. 7. The results of the maximum likelihood analysis, as applied to this sample, are

$$l_\tau = 635 \pm 35 \ \mu m$$

$$R = 1.05 \pm 0.04$$

The expected distribution parameterized by these values is shown superimposed on Fig. 7, and is seen to provide a satisfactory representation of the data.

Contamination of the τ sample with the backgrounds discussed in Sec. 3.2 will tend to reduce the apparent mean decay length. To determine the magnitude of this effect, we combine appropriate amounts of the simulated hadron and two-photon backgrounds with a simulated τ sample of nominal

lifetime, and study the corresponding change in the measured decay length. An alternative technique uses the Monte Carlo events to estimate the mean decay length of each of the background classes, and then considers the effect of the appropriate fraction of each class on the overall mean. The results of the two techniques are consistent, and imply that the presence of the background lowers the result by 31 ± 10 μm. Adding this correction to our maximum likelihood result, we find

$$l_\tau = 666 \pm 37 \ \mu\text{m}$$

where the quoted statistical error has been scaled up by the same fractional amount as the pathlength. With the appropriate correction for initial state radiation, the mean τ total energy is expected to be 13.9 GeV. We then find a τ lifetime:

$$\tau_\tau = (2.88 \pm 0.16) \times 10^{-13} \text{ sec.}$$

The quoted error is statistical; systematic uncertainties are discussed in the next section.

5. Checks on the Analysis

5.1 Measurement Bias

Early measurements of the τ lifetime required substantial corrections to the observed decay lengths to remove a bias which arose from a correlation between the measured decay length and its estimated error. Events with fluctuations toward longer measured decay lengths were associated with smaller track extrapolation errors and thus smaller vertex errors, while fluctuations toward shorter decay lengths were assigned correspondingly larger vertex errors. The former events were consequently

given greater weight in the likelihood fit, biasing the result toward a longer mean decay length.

The improved tracking resolution and reduced multiple Coulomb scattering of this experiment should reduce such bias to a small level. To confirm this, and to check for the presence of other potential systematic effects, we have studied our analysis technique using Monte Carlo generated τ decays. In addition, to check for effects not reproduced by the Monte Carlo, we have made comparisons between tau-like control samples constructed from both real and simulated hadronic events. These studies are discussed below.

5.2 Monte Carlo

Two samples of 20,000 τ decays were created with lifetimes of 0 and 2.80×10^{-13} sec. Each sample is subjected to the complete analysis procedure and maximum likelihood fit. We note here that in the limit in which the mean decay length is very small compared to σ_1, the formula for P_i discussed in Sec. 4.3 poses numerical problems. For the zero lifetime sample, we instead approximate P_i by the Gaussian

$$P_i(l_i, l_\tau) = \frac{\exp\left[-(l_i - l_\tau)^2 / 2(\sigma_i^2 + l_\tau^2)\right]}{\sqrt{2\pi(\sigma_i^2 + l_\tau^2)}}$$

This expression has the same mean and the same RMS deviation as the exact result.

The fit values for the final samples of about 1500 simulated decays at each lifetime are 28±20 μm and 597±22 μm, in good agreement with the mean generated pathlengths in these samples of 0 μm and 612 μm. The fitted

value of R is consistent with unity in each case. Furthermore, in the zero lifetime sample, the distribution of the ratio l_i/σ_i is accurately fit by a Gaussian of unit standard deviation, indicating that, in Monte Carlo events, our analysis does yield a Gaussian error which is well represented by the calculated σ_l.

5.3 Hadronic Control Sample

Having checked the validity of our analysis on a Monte Carlo sample, we need to verify how well the simulation reproduces the experimental environment. For this purpose, we construct, from hadronic events, a control sample which approximately mimics the features of the τ 3-prongs[18] and which, in principle, has a known mean pathlength. Comparison between control samples derived from both real and simulated data will provide a measure of how well the Monte Carlo models the tracking system, as well as set an upper limit on the magnitude of any unanticipated form of measurement bias.

The control sample is selected with the following requirements. The events have 7 or more charged tracks, sum of scalar momenta for all charged particles between 10 and 30 GeV/c, and overall event vertices that are well measured and near the interaction point. A study of tracking χ^2 in these events, similar to that described in Sec. 3.3, indicates that the actual VC resolution is some 30% worse than that for Bhabha tracks. In the same spirit as the discussion of Sec. 3.3, we therefore refit all tracks with the VC error increased by 30%. We then construct "pseudo-taus" by selecting from each event the three highest-momentum, well-measured tracks which have a total momentum between 3 and 15 GeV/c, an opening half angle less than

0.70 radians, and a ratio of total momentum to 3-particle invariant mass greater than 4.0. Tracks are not used if, when combined with any oppositely charged track in the event, the two-particle invariant mass is consistent with that of a Λ^0 or K^0.

The control sample constructed from hadronic data is subjected to the τ selection procedure and the maximum likelihood fit for the mean decay length. The result, using the zero lifetime form, is 156 ± 30 μm, with R = 1.32 ± 0.05.

The same analysis performed on the control sample culled from simulated hadronic events has a fitted mean pathlength of 130 ± 24 μm, with R = 1.14 ± 0.04. The magnitude of the finite pathlength in this sample depends on the values used for the D^0 and D^* lifetimes, the D^0/D^* ratio, and the mean B lifetime. Adding in quadrature the change in the pathlength resulting from reasonable independent variations in these parameters,[19] we conclude that the total pathlength uncertainty expected from these effects is approximately 12 μm.

From this control sample analysis, we make the following observations:

1. The pseudo-tau samples from Monte Carlo and data exhibit good agreement, within the errors, in the fitted mean path lengths. We take this agreement as evidence that any potential offset bias in the τ analysis is limited by the error in the comparison, namely the sum in quadrature of the statistical errors and the error from systematic uncertainties in D and B lifetime effects. The overall estimated uncertainty is thus 40 μm.

2. The Monte Carlo pseudo-tau path length distribution exhibits a larger width than expected, as characterized by the 14% deviation of the scale factor R from unity. We have verified that this effect, as well as the finite mean path length, is entirely associated with the presence of heavy quark decays. It arises from the way in which finite path lengths are generated by the random association of tracks from decays and from the event origin. The distribution of such path lengths is not exponential, and its RMS width is larger than its mean value. The convolution of Sec. 4.3 is thus not an exact representation, and the fit compensates with an R value greater than unity.

3. For pseudo-taus in real hadron data, R is found to be 18% higher than for pseudo-taus in the Monte Carlo. In the case of real τ events, the R value is 1.05 ± 0.4. This is evidence that the widths of the error distributions in the data are larger than anticipated, and that they are larger in hadronic events than in the relatively cleaner τ events. The two parameter fit to l_τ and R, however, leads to a value of l_τ which is less sensitive to the exact shape of the resolution function.

5.4 Summary of Systematic Errors

We find no evidence for significant measurement bias or offset in Monte Carlo study of our analysis procedure. From the comparison of control samples in real and Monte Carlo hadronic events, we assign a systematic uncertainty of 40 μm to such error.

As discussed in Sec. 4.5, the presence of backgrounds in the τ sample lowers the measured mean decay length by 31 ± 10 μm.

We check for the presence of other potential biases by repeating the analysis with independent variations of key parameters. Reasonable changes in the σ_1 cut, the χ^2 cut, and other tracking quality cuts produce no significant variation in l_τ. Use of beam positions derived by an alternate method likewise produces no significant change.[14]

The effect of assuming that the 3-prong exactly follows the τ direction is studied via Monte Carlo simulation. The net difference in l_τ when the true τ direction is substituted for the 3-prong momentum sum is found to be 2 μm, and is thus completely negligible.

We conclude that the potential systematic error of this measurement is given by the sum in quadrature of the bias uncertainty and background error, giving a net systematic error of 41 μm in the pathlength, or 0.17 x 10^{-13} sec in the lifetime.

6. Conclusion

We have used a high resolution vertex detector to measure the lifetime of τ leptons produced in electron-positron annihilation at PEP. The result is

$$\tau_\tau = (2.88 \pm 0.16 \pm 0.17) \times 10^{-13} \text{ sec}$$

where the first error is statistical and the second is systematic. This result is consistent with the theoretical prediction, as well as with other recent experimental determinations.[8] Combining in quadrature both experimental errors and the error on the theoretically predicted lifetime, we find that, at 95% confidence, the strength of the τ coupling to the charged weak current lies within 9% of the universal Fermi coupling strength.

References

1. The form of the lowest order correction to the lifetime is $1 + 8(m_\nu/m_\tau)^2$. The effect of a neutrino mass at the experimental upper limit would lengthen the predicted lifetime by 1.2%. See Y. S. Tsai, Phys. Rev. D4, 2821 (1971) and H. Albrecht et al., Phys Lett. 163B, 404 (1985).
2. Radiative corrections which are not included in the measured value of G_F appear in the form $(m_\tau/m_W)^2$, and are thus completely negligible. See A. Sirlin, Phys. Rev. D22, 971 (1980).
3. P. R. Burchat, in Proceedings of the XXIII International Conference on High Energy Physics, Berkeley, CA, (1986).
4. Particle Data Group, Phys. Lett. 170B, 1 (1986).
5. A. DeRujula in Weak and EM Interactions at High Energy, Les Houches, Session XXIX, 570 (1976).
6. M. Gronau, C. N. Leung, and J. L. Rosner, Phys. Rev. D29, 2539 (1984); X. Y. Lee and E. Ma, Phys. Rev. Lett. 47, 1788 (1981); L. Abbott and E. Farhi, Phys. Lett. 101B, 69 (1981).
7. D. A. Bryman et al., Phys. Rev. Lett. 50, 7 (1983).
8. H. R. Band et al., Phys. Rev. Lett. 59, 415 (1987); C. Bebek et al., Phys. Rev. D36, 690 (1987); S. Abachi et al., ANL-HEP-PR-87-1, April, 1987, submitted to Physical Review Letters.
9. J. A. Jaros in Proceedings of the 1984 SLAC Summer Institute, SLAC Report No. 281 (1985); J. A. Jaros et al., Phys. Rev. Lett. 51, 955 (1983)

10. R. H. Schindler et al., Phys. Rev. D24, 78 (1981).

11. R. H. Schindler, Ph.D. Thesis, Stanford University, SLAC Report No.219 (1979).

12. J. Jaros in Proceedings of the International Conference on Instrumentation for Colliding Beam Physics, SLAC Report No.250, (1982)

13. M. Atac, IEEE Trans. Nucl. Sci. 31, 99 (1984).

14. L. Gladney et al., Phys. Rev. D34, 2601 (1986).

15. The final values for the beam sizes derived from the full data set are $\sigma_{bx} = 423 \pm 14$ μm and $\sigma_{by} = 72 \pm 9$ μm. The small change from the values in Sec. 2.3 has no effect on the measured mean path length. See Ref. 17.

16. P. R. Burchat et al., Phys. Rev. Lett. 54, 2477 (1985); B. G. Bylsma et al., Phys. Rev. D35, 2269 (1987).

17. Rene Ong, Ph.D. Thesis, Stanford University, SLAC Report No.320 (1987).

18. The momenta of the hadronic 3-prong combinations are smaller than those of taus, and the hadronic tracking environment is more crowded.

19. J. C. Anjos et al., Phys. Rev. Lett. 58, 311 (1987); M. G. Gilchriese in Proceedings of the XXIII International Conference on High Energy Physics, Berkeley, CA, (1986); M. Derrick et al., Phys. Rev. Lett. 53, 1971 (1984).

Figures

1. Vertex detector track χ^2 for Bhabha scattering tracks. The fit is the expected form for 5 degrees of freedom.
2. Extrapolated separation distance between Bhabha tracks at the interaction point.
3. Vertex detector track χ^2 for tracks in tau decay 3 prongs, after rescaling the VC resolution by 15%. The fit is the expected form for 5 degrees of freedom.
4. Vertex χ^2 distribution for the fit to the 3 prong vertex in the xy plane. The solid line is the expected form for 1 degree of freedom.
5. Schematic view of the tau decay vertex, showing beam and decay vertex error ellipses. The decay length, as well as the decay and production points are found by the fit discussed in Sec. 4.2.
6. Distribution of σ_l, the three dimensional fitted error in decay length, for the final τ sample.
7. Distribution of l_i, the three dimensional fitted τ pathlength, in the final sample. The solid curve is the result of the fit in Sec. 4.4.

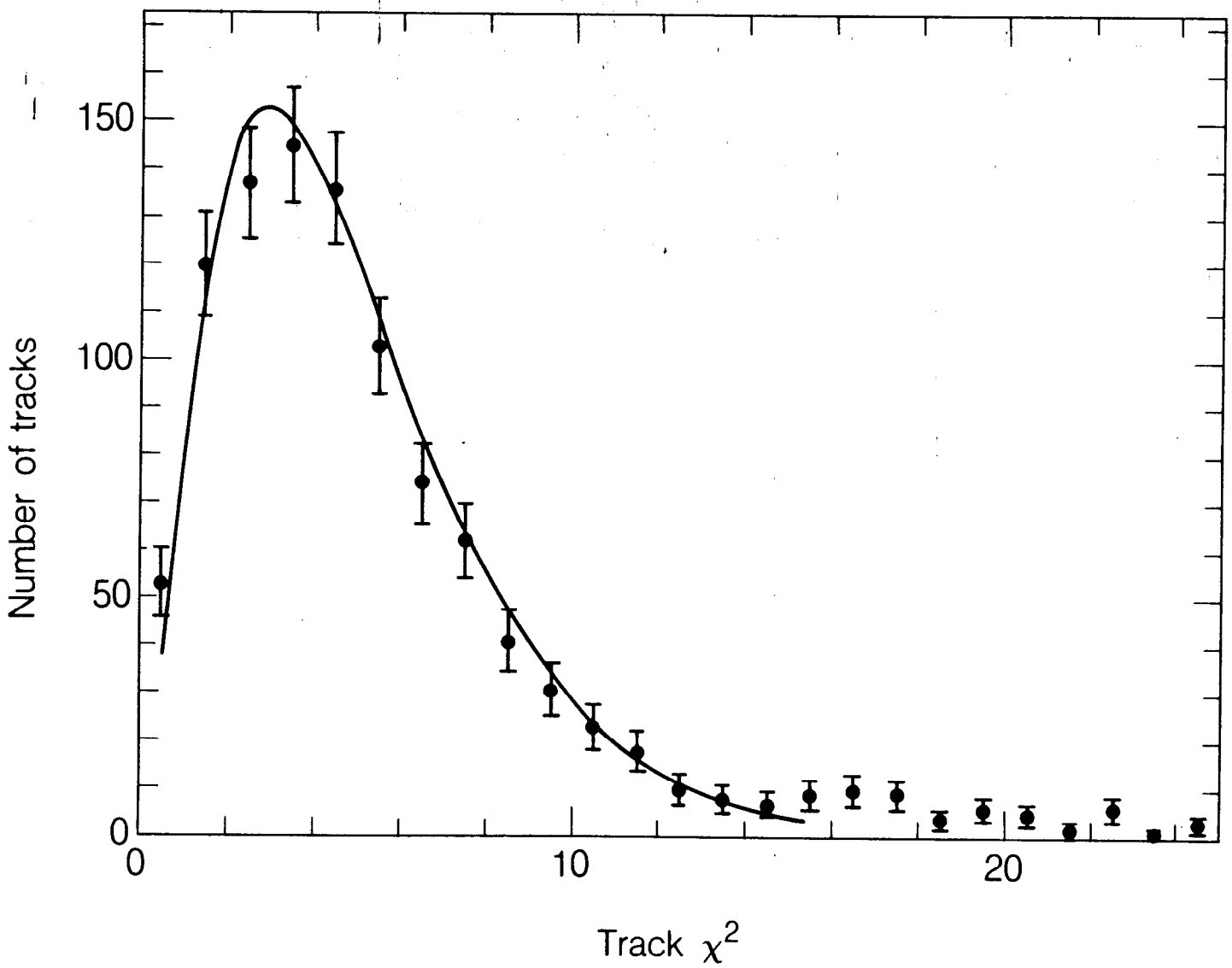

XBL 877-11119

Fig. 1

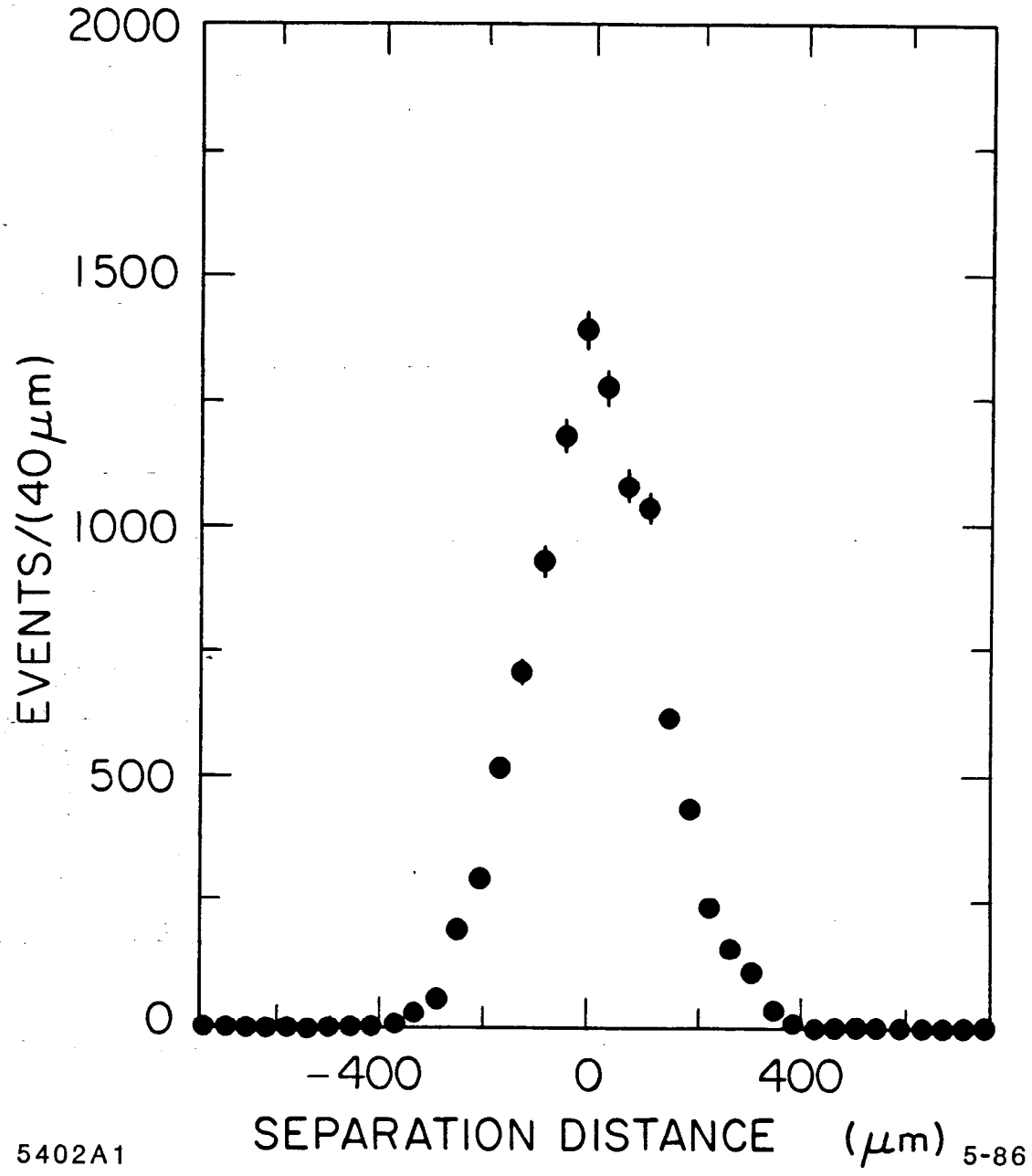
2000
1500
1000
500
0
EVENTS/(40μm)
-400
0
400
SEPARATION DISTANCE (μm)
5402A1
5-86

Fig. 2

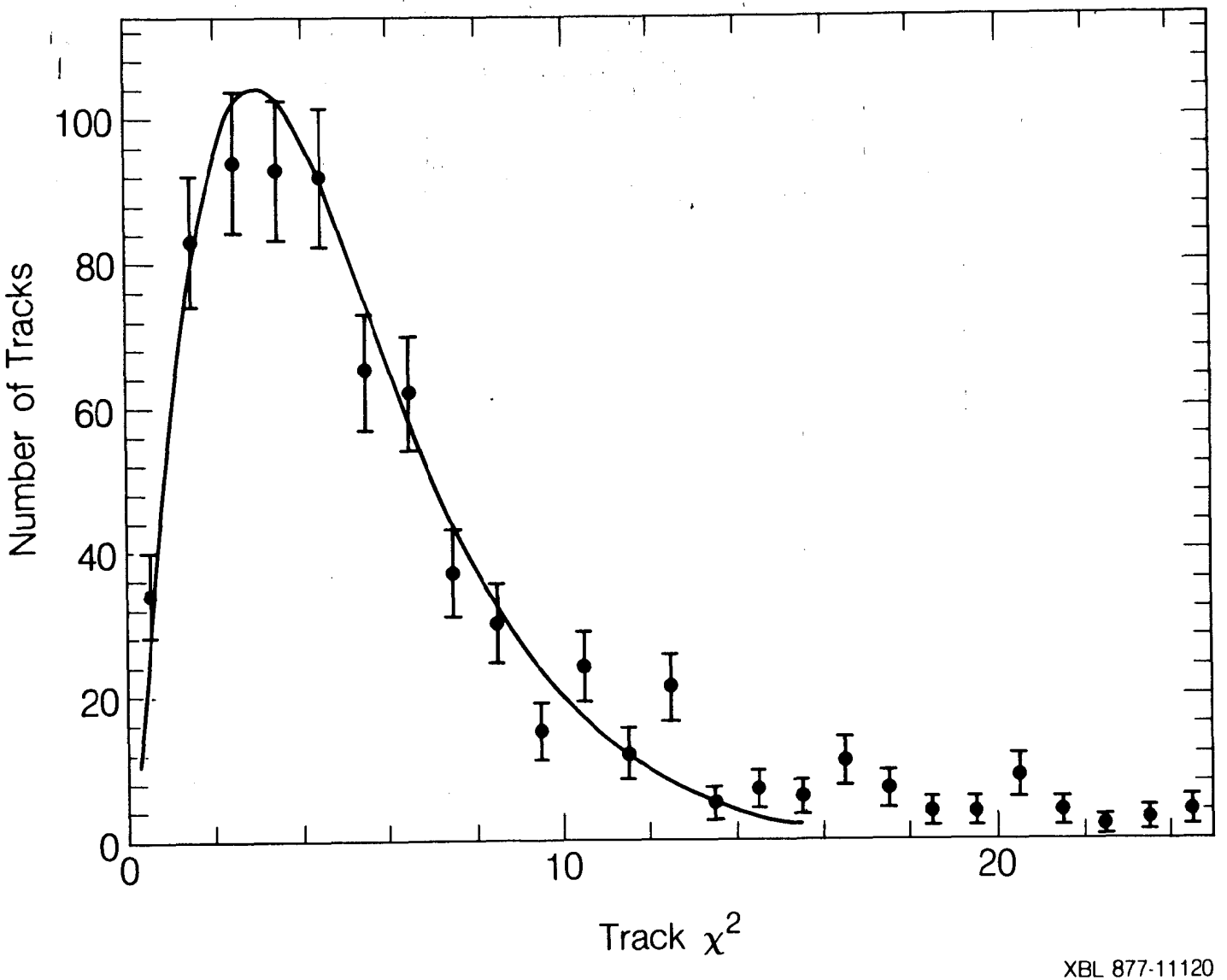
Number of Tracks
100
80
60
40
20
0
0
10
20
Track χ^2
XBL 877-11120

Fig. 3

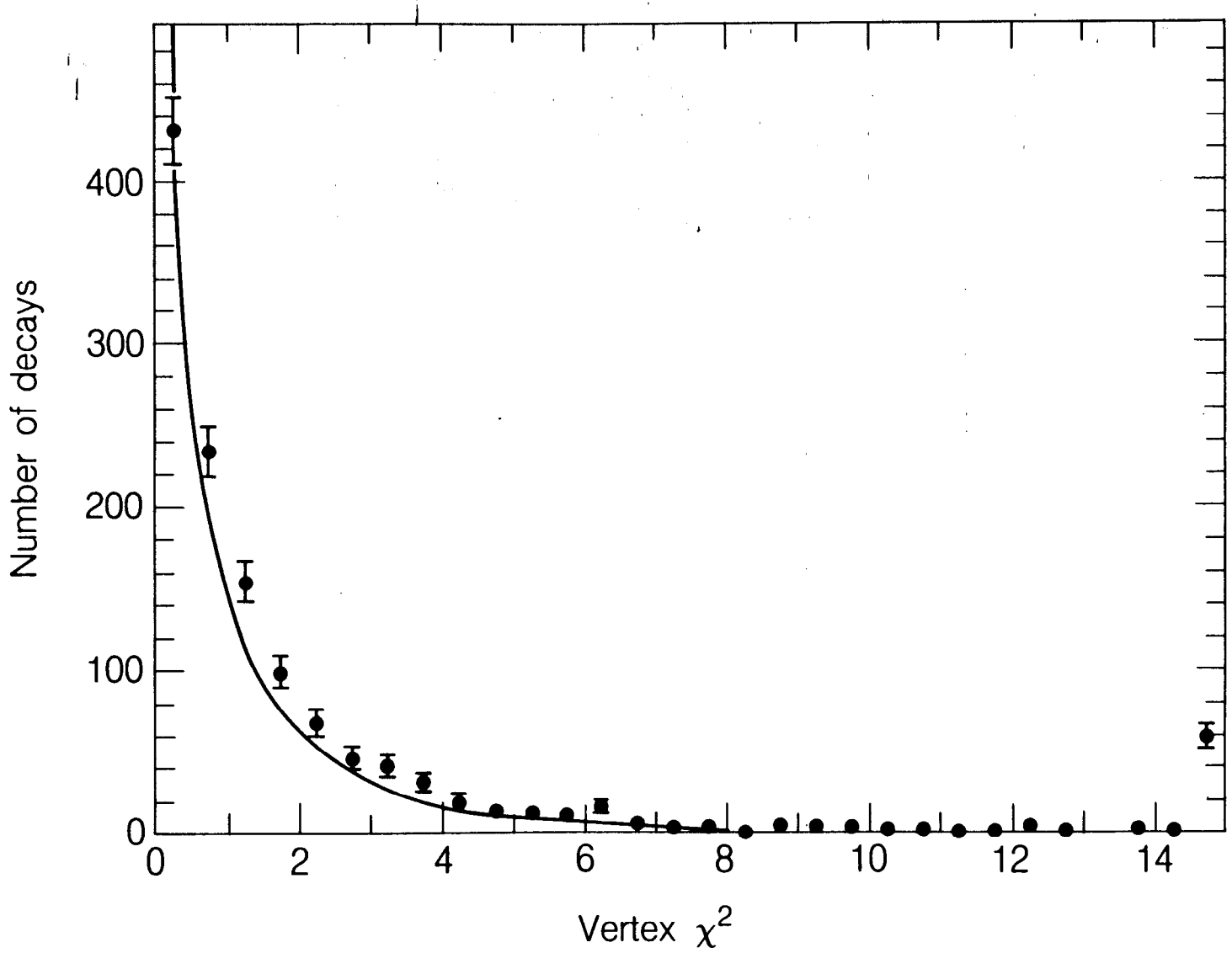

XBL 877-11123

Fig. 4

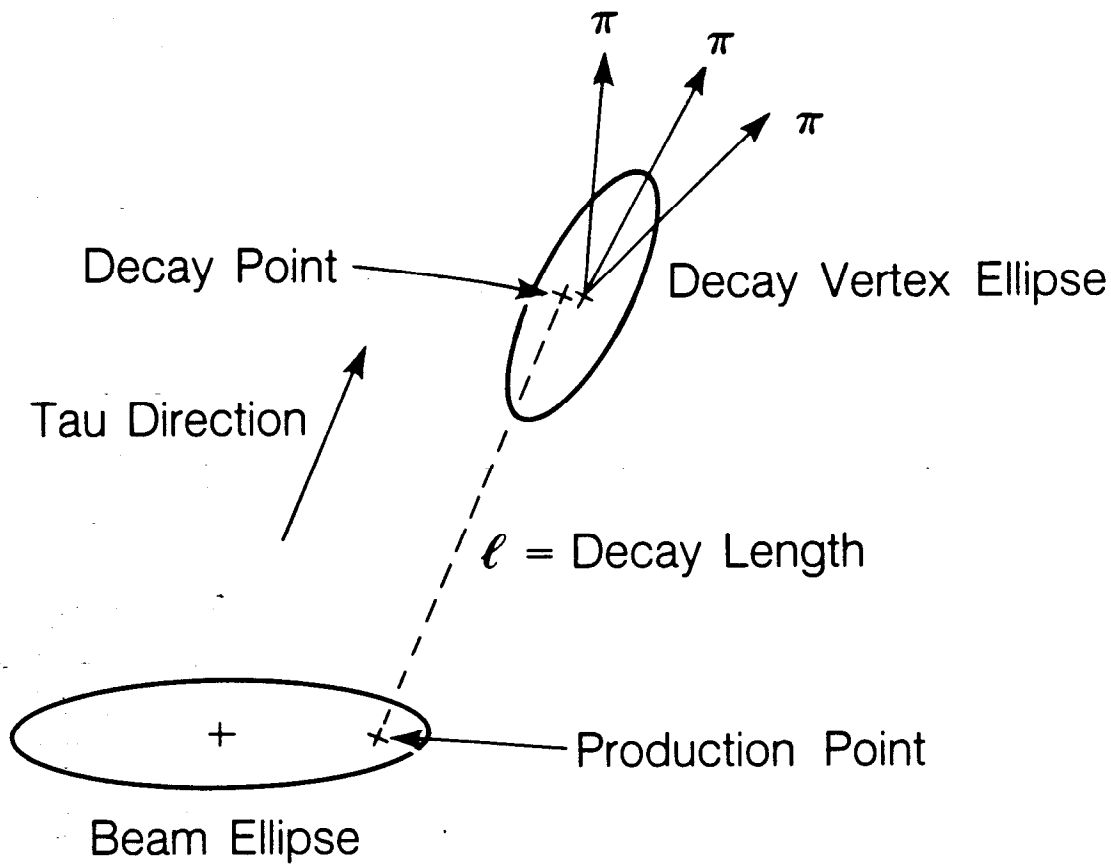

XBL 877-10829

Fig. 5

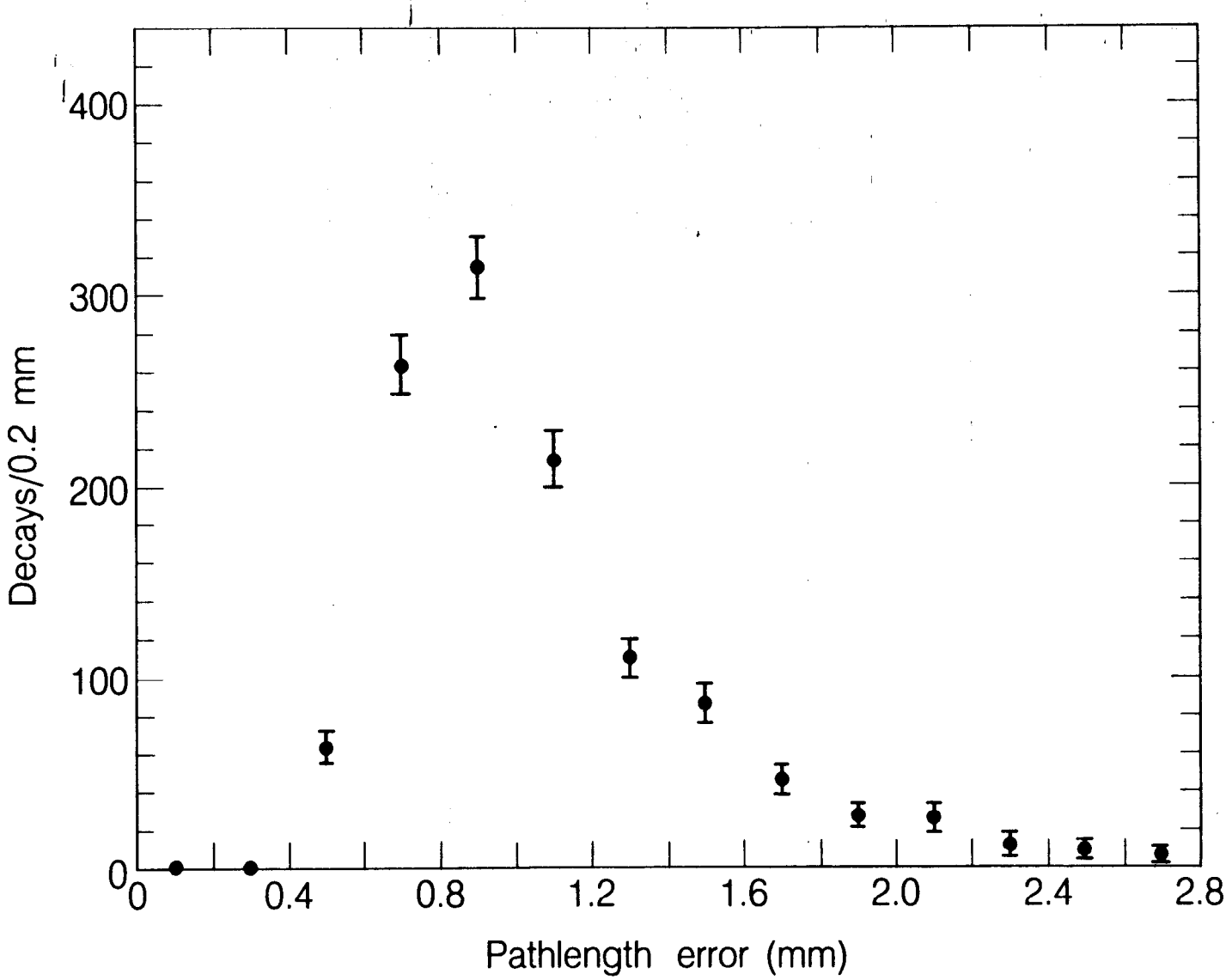

XBL 877-11122

Fig. 6

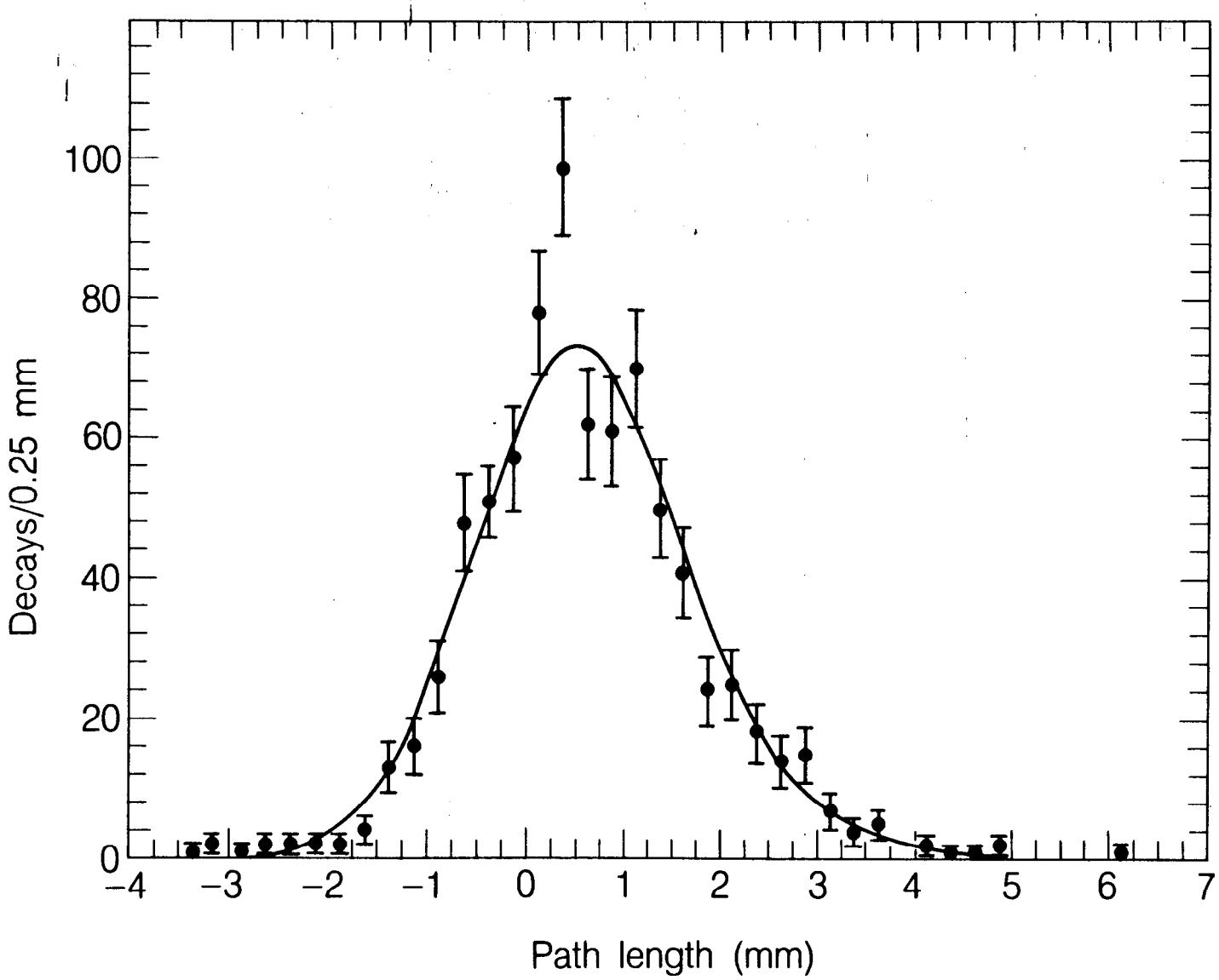

XBL 877-11121

Fig. 7